Effect of silver inhibition on the ceramic foam as flame suppression

Nur Faazila Hamzah[1], *Rafiziana* Md. Kasmani[1*], and *Sheela* Chandren[2]

[1]Faculty of Chemical and Energy Engineering, Universiti Teknologi Malaysia, 81310 UTM Johor Bahru, Johor, Malaysia.
[2]Faculty of Science, Universiti Teknologi Malaysia, 81310 UTM Johor Bahru, Johor, Malaysia.

Abstract. Aluminium dust explosions pose significant safety and economic challenges in various industrial processes. Due to this, the current research explores an innovative approach by inhibiting the silver nanoparticles (Ag NPs) to ceramic porous form substrate as a flame suppressant in order to mitigate the risks associated with these explosions. The antimicrobial and non-toxic qualities of silver are also attractive to be applied in medical and food technology. However, the interfacial adhesion between the metallic (nanosilver) and non-metallic (silica-based-ceramic) is still vaguely studied due to the mechanical and surface energy mismatch between the organic surface and the inorganic layers. From this study, the physicochemical and mechanical properties of the silver-coated ceramic foam were analyzed using X-ray diffraction, field emission scanning electron microscopy with energy dispersive X-ray, thermogravimetric analysis, and compression test. From the mechanical testing, it was found that the percentage increase of maximum load for silver-ceramic foam from the original ceramic foam was about 60%. The results indicate that silver-coated foam has a better compressive strength of 0.93 MPa as compared to 0.58 MPa by the original ceramic. The inhibition effect of Ag NPs powder on the explosion pressure evolution and flame spread mechanism of aluminium powder at different concentrations and particle sizes was tested using the Hartmann experimental system.

1 Introduction

In contrast to gas explosions, dust explosions emit greater energy and produce high-temperature and high-pressure substances, often resulting in numerous accidents. The intricate reaction processes involved in dust explosions heighten the challenges in their prevention, and certain secondary explosions exacerbate the extent of damage caused by accidents [1,2]. The processes of producing aluminium products are usually accompanied by large amounts of aluminium dust, which might induce serious aluminium dust explosions and cause severe casualties [3,4]. Over time, dust explosions have increasingly become a prevalent type of incident across various industrial sectors. This presents a significant menace to effective production processes and results in substantial losses in terms of both human lives and property [5–7]. Because of the rising frequency of dust explosion incidents, researchers have delved into the combustion mechanisms, flame propagation characteristics, and preventive technologies associated with dust explosions. Numerous studies indicate that the occurrence of dust explosions is influenced by various factors, including the physical and chemical properties (such as particle size, concentration, moisture content, and devolatilization), as well as certain initial conditions (like initial temperature and pressure, and ignition energy) [8–10].

To mitigate and manage dust explosions, one can disrupt the "dust explosion pentagon" [11]. A noticeable inerting effect arises from the reduction in dust and oxidant concentrations. Studies have revealed that various inert solid powders like phosphate, silicate, carbonate, and silicon dioxide effectively hinder explosive reactions in dust [12–14]. Chen et al. [15] observed that sodium bicarbonate powder significantly suppresses flame propagation in aluminium, resulting in reduced flame velocity and a disrupted flame structure. During the storage and transportation of combustible dust, incorporating inert solids or gases has proven effective in reducing the risk of explosion accidents. When inert techniques fall short, it becomes crucial to focus on methods that impede the propagation of explosion flames, thus minimizing accident-related losses. Porous materials have garnered attention from researchers due to their significant specific surface area, which aids in extinguishing explosion flames. However, the application of porous materials in explosion control has primarily been restricted to combustible gases. For instance, ceramic foams, a typical porous material that not only serves functions like filtration, adsorption, and catalysis [16–18] but also has the capability to inhibit gas explosion reactions [19,20]. In some cases, certain parameters associated with porous materials might even intensify explosion pressure. For instance, when mesh aluminium alloys were employed in hydrogen/air mixture explosions, they proved ineffective in

* Corresponding author: rafiziana@utm.my

suppressing the explosion, and instead, the maximum explosion pressure increased [21].

Given the pressing demand for industrial safety, addressing and reducing the risks associated with dust explosions have become the primary concern at present. Enhancing the safety of dust-related processes hinges on the development of inhibition technologies aimed at preventing explosions from spreading or escalating. One particularly promising approach for suppressing explosions, both economically and environmentally friendly, is the advancement of explosion suppression technology involving the use of porous materials. The effectiveness of this method primarily relies on the characteristics of the substances used to suppress explosions and how evenly they are distributed within the area prone to explosions. Ceramic foam, with its combination of high porosity and a large specific surface area, has been found to possess an interconnected micro-network structure that contributes to extinguishing gas explosion flames and mitigating shock wave overpressure [19]. While ceramic foam has been proven effective for fire prevention and explosion suppression in the context of gas explosions, its application in dust explosions has been relatively scarce. Furthermore, ceramic foams are known for their inherent brittleness, making them less suitable as explosion suppression materials, especially in aggressive environments characterized by high temperatures and pressures. To address this issue and enhance the mechanical strength of ceramic foam, this study introduces a novel approach: the application of a metal nanoparticle coating. This initiative aims to modify the physicochemical properties of the foam, thereby reinforcing its structural integrity and durability, ultimately offering a dual solution for explosion suppression.

Based on the previous work done by Mokhtar et al. [22], it was confirmed that nanosilver particles have a suppressing effect in lowering the overpressure during aluminium-dust explosion and this could be an excellent candidate as a suppressing agent with high thermal and mechanical properties in semiconductor, gas burner filtration, space shuttles, etc. Therefore, in the current study, the non-precious metal of silver was chosen as the coating powder, considering its good electrical conduction and thermal abilities. Due to the robustness of the ceramic foams to withstand high temperatures and aggressive environments, it is hypothesized that modification of the ceramic foam with silver metal could reinforce the mechanical properties to withstand mechanical impact and higher mechanical loading. Since both ceramic (non-metallic) and metallic nanopowder coating have representative significance, it will be our interest to explore the synergetic effect of metal deposition on the ceramic foam when combined, it gives higher porosity, mechanical stability, higher heat resistance, and adhesion to the ceramic support and thus, minimize the blocking due to the smaller microchannels. The purpose of this work was to investigate the inhibition effect of silver metal on aluminium dust explosion. On the one hand, the synergetic effect of metal inhibition on coated metal-ceramic foam for explosion parameters (Pmax and dP/dtmax) and quenching behavior on aluminium powder vented explosion was quantitatively examined via a designed aluminium dust explosion experimental system in a 1.2-L vertical vessel at various concentrations. Moreover, the inhibition mechanism was discussed in depth at the end of this paper. This paper not only proves the great inhibition effect of silver nanoparticles (Ag NPs) in explosion suppression, but the research results will also aid in improving the intrinsic safety of the metal-processing industry and reducing the hazards of dust explosions.

2 Materials and Methods

2.1 Materials and Chemicals

The main porous element used in this study is white alumina porous ceramic foam was purchased from Pingxiang Bestn Chemical packing) with a thickness of 25 mm, a diameter of 70 mm and a pore size of 60 pores per inch (ppi). Silver (Ag) and aluminium (Al) powder with a particle size of 70 nm and 99.8% purity, were purchased from Hongwu International Group Ltd., China. All materials and reagents used in this work were of analytical grade as tabulated in Table 1. The aqueous solution used was distilled water.

Table 1. List of materials and chemical reagents

Materials/Chemical reagents	Molecular formula	Brand (Purity)
Acetone	CH_3COCH_3	MERCK (99.5%)
Ethanol	C_2H_5OH	VChem (95%)
Polyvinylpyrrolidone (PVP10)	$(C_6H_9NO)_n$	Aldrich (99%)
Absolute ethanol	C_2H_6O	MERCK (99.98%)
3-Aminopropyltrimethoxy silane	$C_6H_{17}NO_3Si$	Aldrich (97%)

The current work focuses on silver with a particle size of 70 nm as well as the aluminium dust powder. This was based on the findings obtained by Mokhtar et al. [22] where 70 nm aluminium particles were homogeneously distributed, whereas 40 nm Al particles exhibited agglomerations due to the intermolecular forces in accordance with the smaller surface area as shown in Fig. 1. The use below the 70 nm particle size made the agglomerations become more severe and might not be suitable for use in the current application. Therefore, 70 nm was chosen as the best particle size in this study.

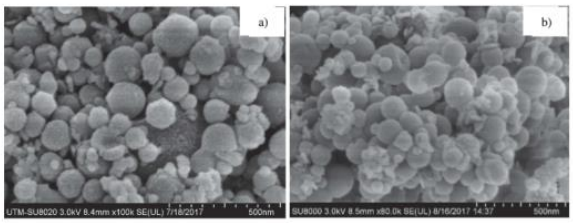

Fig. 1. Morphology of (a) Al 70 nm and (b) Al 40 nm particles before explosion

2.2 Materials and Chemicals Sample Pre-treatment and Modification by Silanization Agents

Alumina (Al_2O_3) porous ceramic foams with dimensions of 70 mm diameter x 25 mm thickness were first pre-treated by sonicating with acetone and then rinsed with ethanol and distilled water each for 15 minutes respectively before drying overnight in an oven at 60 ºC by referring to Luo et al. [23] with slight modifications. Surface modification was done on the ceramic foams by treatment with 3-aminopropyltrimethoxy silane (APTMS). This was carried out by dissolving 0.0275 mol of APTMS in 250 mL of absolute ethanol. The substrate was immersed in the APTMS solution for 1 h at room temperature in ultrasonic. The foam was then removed from the APTMS solution, and rinsed with adequate amounts of ethanol and distilled water respectively. The foam was dried overnight in an oven at 60 ºC This method was modified accordingly based on a previous study using polycarbonate material [24]. The schematic diagram of the sample pre-treatment and surface modification using APTMS is illustrated in Fig. 2 below:

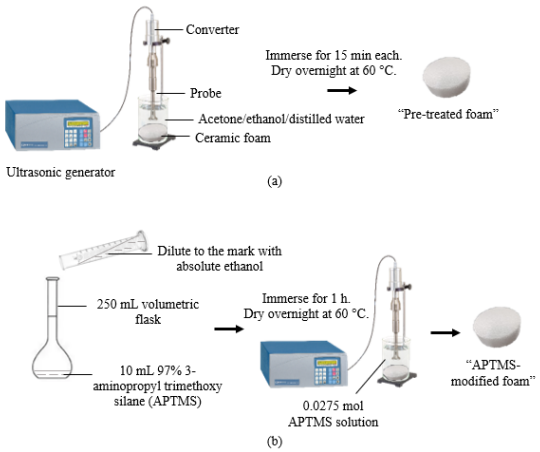

Fig. 2. Schematic diagram of (a) sample pre-treatment and (b) surface modification using APTMS

2.3 Dispersion of Silver Nanoparticles

In this study, silver (Ag) powder was purchased in the form of metallic nanopowder with a specific size of 70 nm and the size was controlled by dispersing Ag powder through ultrasonic dispersion in a solvent containing a surface stabilizer before the coating process was done onto the ceramic substrates. 10 g of nanopowder was dispersed in 200 mL absolute ethanol. The resulting solution was stirred gently. The particle size was observed. If it agglomerates, 1–2% PVP (MW 10,000) will be added dropwise. The desired particle size of the Ag NPs coated on ceramic foam is expected to be between 70 – 100 nm. Fig. 3 shows the summarised procedures for the Ag powder dispersion.

Fig. 3. Schematic diagram for dispersion of silver nanopowder

2.4 Deposition Technique Used

The deposition technique applied was spray-coating. Based on a previous study by Hamzah et al. [25], the spraying method successfully deposited nickel nanoparticles on ceramic foam in the presence of silanization agents of APTMS to enhance the binding of such metal onto the surface of the ceramic foam. Hence, silver nanoparticles were coated onto the ceramic foam in the presence of silanization agent of APTMS in such a way that the coating would bind in the same manner as nickel. The APTMS-modified foams were coated with silver solution by spraying directly onto the stable surface of the ceramic foam by using an F-75(S) commercial air spray gun with a nozzle size of 1.5 mm at a distance of 15 cm. To ensure uniform coating, careful steps should be taken; here, the number of coating layers was standardized to 4, the gap between the nozzle spray head and the ceramic foam surface was maintained at 20 cm, and the air pressure was maintained between 70 and 100 kPa. The coated foams were further heat-treated at 80 °C [25]. Fig. 4 illustrates the procedures for the spray-coating of Ag nanopowder.

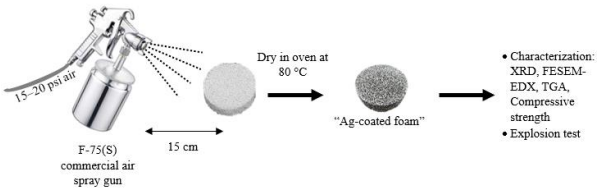

Fig. 4. Schematic diagram for spray-coating of Ag powder

2.5 Characterization Methods and Instruments

The Ag-coated ceramic foams were analyzed in terms of their physicochemical properties as well as their mechanical strength. Several characterization methods were used for the pre-explosion and post-explosion foams, which are X-ray diffraction (XRD), Field Emission Scanning Electron Microscopy with Energy Dispersive X-ray (FESEM-EDX), thermogravimetric (TGA) analysis and compressive test. The crystallinity

and phase content of the prepared coating films were determined by XRD using Rigaku SmartLab X-Ray Diffractometer operated at 40 kV and 30 mA with a scan speed of 4°/min. Composite samples were ground and spread on the sample holder and measurement was carried out in the 2θ range of 20° to 80°. Morphological studies of metal NPs were carried out by FESEM (JSM-7600F, JEOL, Tokyo, Japan) at 5.0 kV accelerating voltages with the magnification of 35×, 10,000×, and 50,000×. The surface of the metal-coated ceramic foam was coated with platinum prior to the investigation using the sputtering technique to avoid electron charging on the sample surface. EDX is employed to characterize the elemental compositions, abundance, and purity of the nanoparticles. Furthermore, the EDX spectra were also acquired to detect the C, O, Al, Si, and Ag elements. Further, thermal analysis of the coated ceramic foams will be performed by TGA at a rate of 30 °C/min from 30 °C to 1000 °C under purified air. Last but not least, compressive mechanical testing will be carried out by using the universal testing machine (Instron 5982) with a crosshead of 0.5 mm/min to provide information about the maximum compressive strength of the silver-coated ceramic foams to be compared with the previous study using the original ceramic and nickel-coated ceramic. The post-explosion samples were analyzed for their morphologies, crystallinity, phase content and elemental composition to determine the amounts of silver oxide produced after the powder explosion test. This was used for comparison purposes with the pre-explosion samples.

2.6 Experimental Set-Up

The powder explosion test was performed in a 1.2-L stainless steel cylindrical test vessel with an internal diameter of 70 mm and a height of 304 mm as illustrated in Fig. 5. The experimental studies involved aluminium powder in a nano-sized (70 nm) used as the fuel in determining the explosion parameters of aluminium powder at different powder concentrations ranging from 300 – 1200 g/m3. A filter paper with a diameter of 125 mm is only considered as a vent cover for the venting explosion in this work. The installation of silver-coated foam in a vented explosion has been adopted for the quantification of the synergetic effect of metal inhibition on coated metal-ceramic foam for explosion parameters and quenching behavior on aluminium powder explosion and compared to that of the non-coated foams and nickel-coated foams. As such, the double suppression system will be adopted in this work, for which filter paper will be used as a vent cover together with the ceramic foam to evaluate the effectiveness of flame quenching of metal dust explosion. The aluminium powder samples were weighed based on their concentrations and particle sizes. Eq. 1 is the formula to calculate the mass of aluminium powder sample:

$$m = MV \quad (1)$$

where;
m – Mass of aluminium powder (g)
M – Concentration of aluminium powder (g/m3)
V – Volume of chamber (m^3)

Concentrations of aluminium powder are between 300 – 1200 g/m^3, following ASTM E1226 (Standard Test Method for Explosibility of Dust Clouds). This test method provides a procedure for performing laboratory tests to evaluate the deflagration parameters of dust. The silver-coated ceramic foam was placed in the vessel chamber slightly below the pressure sensor, whilst filter paper was mounted on the top of the vessel as a venting membrane. The metal powder was placed in the dispersion cup and the test vessel was tightened up. The valve was opened from the air compressor and the compressed air bottle was filled until the pressure read up to 6 bar. The valve from the bottle to the vessel must be closed. After filling up the compressed air bottle, let the airflow to the vessel by opening the valve. The sample was dispersed by compressed air at a pressure of 6 bar. All the systems must be in a ready mode (Data acquisition and LabVIEW system). After the dispersion, the sample was ignited by a centrally mounted igniter, following a 60-ms time delay. The software was operated and the igniter capacitor (10 J) was switched on continuously. The explosion pressure evolutions were measured by a piezoelectric pressure transducer (Keller Series 11, with accuracy ± 0.001 s). The running software was stopped. The main switch was turned off and all the connectors to the igniter were unplugged. The data yield of the experiment was recorded by a data acquisition system from National Instruments with a sampling rate of 100 MHz. Each test was performed in at least three replications for accuracy and reproducibility. The resulting data yielded maximum explosion pressure (Pmax) from the pressure–time profiles. Further, the maximum rate of pressure rise (dP/dtmax) was calculated based on the tangent of the pressure–time profiles [26]. The current findings were then compared to that of the Pmax and dP/dtmax of the original foam.

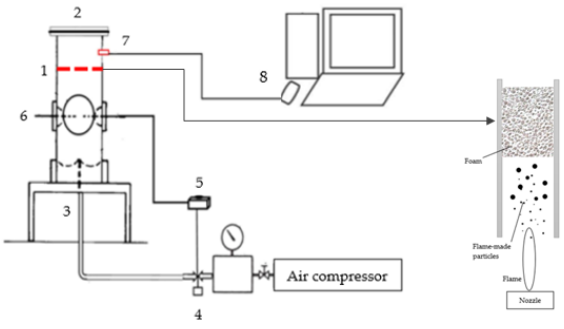

Fig. 5. Experimental apparatus: 1. Ceramic foam, 2. Venting membrane, 3. Gas nozzle, 4. Solenoid valve, 5. Time controller, 6. Igniter, 7. Pressure transducer/sensor, 8. Data acquisition system.

3 Results and Discussion

3.1 Morphological Analysis by FESEM

The results of the FESEM analysis before and after the explosion for the silver-coated ceramic foam at different magnifications of 35×, 10,000×, and 50,000× are presented in Fig. 6. The agglomeration effect of aluminium and silver powder is more pronounced after the explosion as demonstrated in Fig. 6(b), implying that the mass burning rate is significantly reduced due to the smaller specific area, hence justifying the lower Pmax shown in Fig. 11(b). The mechanism involved was the intraparticle agglomeration of both aluminium and silver nanoparticles of the same purchased particle size of 70 nm. From the picture, it is quite difficult to differentiate both nanoparticles at a glance. However, based on a previous study by Mokhtar et al. [22], they found that both metals tend to agglomerate with each other, causing larger effective particle sizes. From the current study, the size of the nanoparticles after the explosion ranges from 81 – 205 nm. The findings revealed that the silver NPs coated on ceramic foams are non-uniform with obvious agglomerations of metallic-silica present on the strut structure. The morphological structures of aluminium powder are consistent with the literature [27,28] which reported that the aluminium morphology is formed as a result of the condensation of gas-phase reaction. The agglomeration effect, which tends to occur in nanodusts, is attributed to the insufficient aerodynamic forces to obstruct the interparticle attraction and subsequently inhibit the dispersion of particles into a primary particle cloud [29,30].

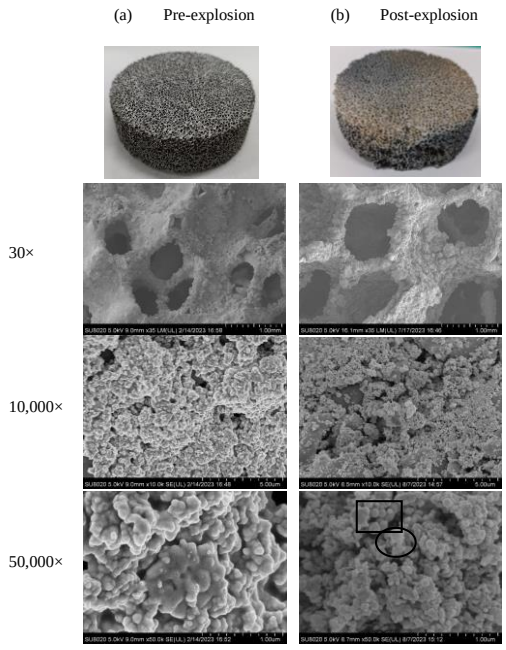

Fig. 6. FESEM micrographs of Ag NPs (in rectangle) on ceramic foams, (a) before and (b) after Al nanodust (in circle) explosion at different magnifications corresponding to Figure 4.17(c).

In addition to silver having a higher molar mass and being a less reactive metal compared to aluminium, the agglomeration of particles seems to be more favorable in the case of silver-coated foams compared to uncoated foams, as confirmed by FESEM analysis. This agglomeration phenomenon could have an impact on the overall pressure development. It is plausible that the likelihood of particle agglomeration between silver nanoparticles on the foam's surface and the aluminium powder increases with higher concentrations of aluminium powder used. As a result, the oxidation of aluminium particles becomes challenging due to the reduced surface area available for the oxidation reaction and the slower oxidation kinetics.

3.2 Surface Elemental Analysis by EDX

The preliminary characterization using EDX analysis to determine the best coating technique for use in the application based on the detection of Ni NPs can be found elsewhere [25]. Fig. 7(a) displays the EDX spectrum for the pre-explosion sample of silver-coated ceramic (denoted by S1), while Fig. 7(b) presents the EDX spectrum for a post-explosion sample of silver-coated ceramic (denoted by S2). For S1 and S2, the elements observed were similar to that of the original alumina foam (Al, O, C, Si) with the additional element of silver (Ag) since silver was used as the coating powder on ceramic foam. It can be seen that the amount of silver in S1 shows an obvious reduction of approximately 63% due to the oxidation of silver into silver oxide (Ag_2O). The presence of such oxide can be seen in the XRD diffraction spectrum in Fig. 8 for sample S2.

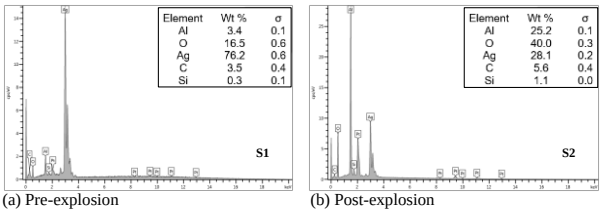

(a) Pre-explosion (b) Post-explosion

Fig. 7. EDX spectra of silver-coated ceramic (S1/S2)

3.3 Crystallinity Study by XRD

The preliminary characterization to determine the crystallinity of the APTMS-modified sprayed samples of nickel-ceramic foam was determined by XRD based on the previous work [25]. It was found that 80 °C was the suitable temperature for the metal coating. Therefore, such temperature was used for the coating temperature of the silver NPs onto the ceramic foam. XRD pattern for the pre-explosion of silver-coated ceramic foam shows characteristic peaks comprised primarily of corundum (Al_2O_3) and some cristobalite (SiO_2) phases which made up the alumina. The same peaks were observed after the aluminium powder explosion. There were no obvious changes in the crystalline structure of the foams as the alumina was present in pure powder form same goes for the silver powder. The XRD patterns of S1 in Fig. 8 indicated that the structure of Ag NPs is face-centered cubic (FCC). In addition, all the Ag NPs had a similar diffraction profile,

and XRD peaks at 2θ= 38.1°, 44.3°, 64.4° and 77.4° could be attributed to the (111), (200), (220) and (311) crystallographic planes of the face-centered cubic silver crystals, respectively [31]. The XRD pattern thus clearly illustrated that the Ag NPs (S1) denoted by the symbol (■) formed in this study were crystalline in nature. The main crystalline phase was alumina with a trace of Ag NPs as impurities were found in the XRD patterns. Fig. 10(b) shows the XRD pattern of silver oxide (Ag_2O) NPs (S2) sintered at 80 °C. All the diffraction peaks of (111), (200), (220), and (311) denoted by the symbol (▲) can be well matched with the cubic phase structure with pattern peaks at 2θ = 38.0°, 44.2°, 64.3°, and 77.1°. Hence, all the reflected peaks in this pattern were found to match with the silver oxide phase having face centered cube (FCC). The broadened peak shows the nanometer-sized crystallites. The structure of the resultant data is well-matched with the standard reference data card no. 01-071-4613.

The appearance of these peaks showed no significant changes before and after the explosion. This could be due to the agglomeration of the particles involved in the oxidation during the explosion of aluminium powder. However, not all the silver NPs in S2 have been oxidized completely upon explosion. This could be seen in the crystal planes of S2, where planes (111), (200), (220) and (311) show only a slight increase in the height of the peak from S1. This could be attributed to the low degree of oxidation, resulting in the crystal structure being maintained as FCC. The findings are coherent with the TGA for silver in Figure 9. Since the FCC crystal structure of silver is characterized by closely packed atoms in a three-dimensional arrangement, it results in a relatively lower surface area per unit volume compared to other crystal structures, such as irregular or amorphous ones. In an explosion, where combustion occurs on the particles' surface, having a lower surface area can lead to a decreased rate of combustion. This could be due to fewer exposed sites for chemical reactions to take place, slowing down the overall burning process. In addition, the FCC structure of silver NPs can offer an increase in chemical stability as compared to other structures. This condition could reduce the reactivity of the material and inhibit rapid combustion reactions. In the case of an Ag–Al explosion, a more stable crystal structure for the silver component might slow down its reactivity with aluminium, thereby decreasing the overall burning rate. Further, the crystal structure of silver also provides specific adsorption sites on the coated alumina foam surface. During an aluminium dust explosion, various reactive species such as aluminium particles, oxygen, and reactive intermediates are present. The FCC structure can selectively adsorb certain species, such as oxygen molecules or reactive radicals, more readily than others. The structure of the resultant data is well-matched with the standard reference data card no. 01-071-4613.

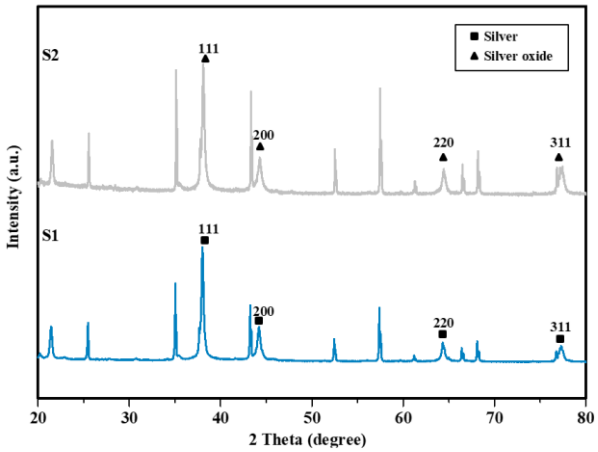

Fig. 8. XRD patterns for pre-explosion (S1) and post-explosion (S2) of silver-coated ceramic foams

3.4 Thermal Analysis by TGA

Thermogravimetric Analysis (TGA) was performed to investigate the thermal behaviour of the ceramic foam together with Ag NPs coated on it. The TG/DTG analysis carried out under air atmosphere was plotted in Fig. 9, showing the percentage weight loss of samples which is represented by TG% as a function of heating temperature. The TG curve for silver-coated alumina foam showed an almost similar trend as the typical alumina foam which can be found elsewhere, but ended with constant weight (no further weight loss observed) that might contain inorganic elements including silica. The DTG curve showed many material losses observed up to 600°C. This could be due to the silver reacting with the surrounding air to give metal oxides in different states. There is almost no weight loss observed above 600 °C. It can be generally attributed to the evaporation of water and organic components. Overall, it can be said that alumina ceramic foam is thermally stable even at high temperatures and it is suitable for use under high-temperature environments. It is well known that the melting point of silver (~960 °C) is much lower than that of the metal used in the previous study which is nickel (~1455 °C). However, when the metal nanoparticles combined with the outstanding feature of the alumina ceramic foam, it would eventually turn into its respective oxide when exposed to high-temperature environments especially when air is present. Hence, the combination of the metal (Ag) with ceramic is expected to give a significant reduction in the overpressure during an explosion. These findings could be supported by the

EDX and the pressure-time profile for Ag-coated ceramic foams.

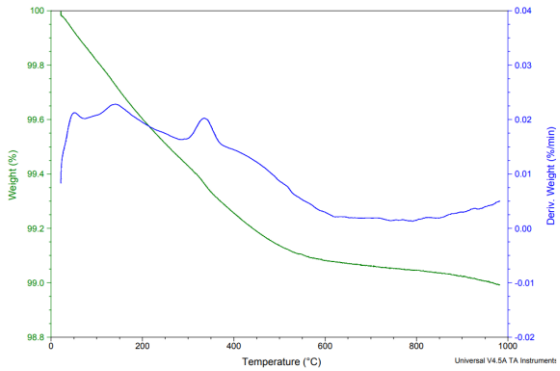

Fig. 9. TG/DTG spectrum for silver-coated ceramic foam operated at the temperature range of 30 – 1000 ℃ and at a heating rate of 10 ℃/min under purified air

3.5 Compressive Strength by Universal Testing Machine (UTM)

In this study, the compressive strength outcomes of silver-coated ceramic foam denoted by S1 were characterized by an initial linear phase followed by a long distance of plateaus due to the progressive collapse of the structure. Consequently, we confirm that it is possible to enhance the strength of the ceramic foams by the addition of metal nanoparticles through coating. Fig. 10 shows the typical load versus extension curves, where all the samples showed a linear part followed by an abrupt drop of the applying load corresponding to a brittle failure. In the initial stage, the load increased linearly. This corresponds to the linear elastic behaviour for the typical fracture of brittle foams. When the applied load exceeded a given value the sample started crushing and struts began failing prior to attaining the maximum stress (presumably weaker struts or those aligned in a favourable direction for maximum stress). The compressive strength was determined from the point in the chart recorder where the load reached its maximum indicated by the (▲) symbol. At the crushing point propagation of macroscopic cracks has resulted in a load drop. Additional deformation of the foam occurs as the sample becomes progressively damaged (layer by layer) from either the top or the bottom owing to breakage of struts. It was observed that struts were failing prior to attaining the maximum stress and that the failure of these struts was accompanied by slight drops in the load/extension curve. As noticed the compressive strength was not associated with the failure of a single strut but rather with the propagation of either a macroscopic crack or multiple cracks after damage accumulation has reached a critical level.

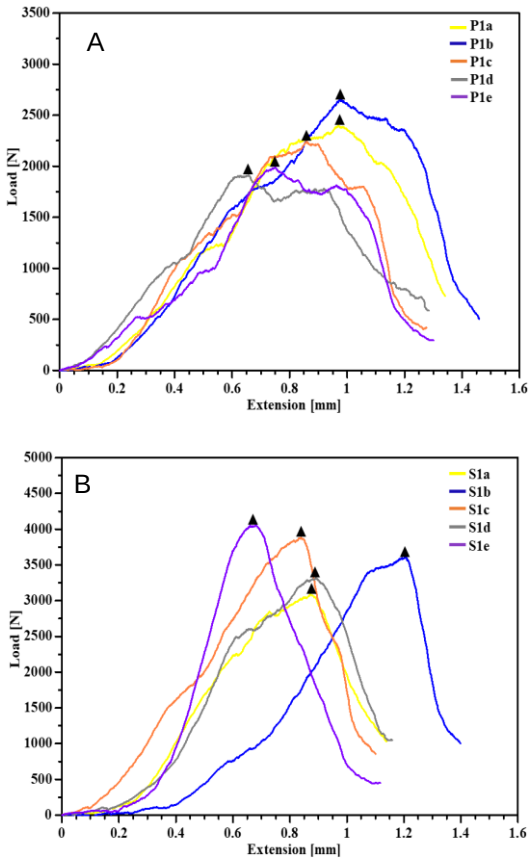

Fig. 10. Graph of load vs. extension for (A) original ceramic and (B) silver-ceramic at crosshead of 0.5 mm/min

As seen from Fig. 10(B), it was found that the silver-coated ceramic foam showed the highest load applied with an average of 3588.56 N at 0.90 mm compression extension. The results obtained experienced a significant increase in the percentage of the load required before foam failure, whereas the original alumina foam in Fig. 10(A) attained the foam's shape up to 0.84 mm extension with 2237.50 N of loads. The percentage increase of maximum load for silver-coated ceramic foam from the original ceramic foam was about 60%. This test was conducted in order to compare the strength of the foams before and after being coated with silver nanoparticles. From the result obtained, it can be found that sample S1 had the highest average compression strength value of 0.93 MPa with the shortest deformation of plateau due to the small and uniform pores of the samples. Meanwhile, P1 showed the lowest compression strength of 0.58 MPa due to the presence of a large pore diameter. As explained by Yu et al. [32], the larger diameter of the cell size will produce inhomogeneity of density and the stress drop ratio will develop into larger. Table 2 shows the summary for all three foams' maximum load, compression extension, compression stress, and compression strain in accordance with their respective average pore diameter. The smaller the diameter of the pores, the higher the compressive strength of the ceramic foams. This could be due to the densification between the metal nanoparticles of nickel and silver deposited on the porous structure of the original alumina ceramic.

Table 2. Summary of compression test for the original ceramic foam (P1) and silver-coated ceramic foam (S1) with their respective pore diameter.

Specimen	Pore diameter [mm]	Load [N]	Extension [mm]	Stress [MPa]
P1a	0.952	2397.894	0.968	0.623
P1b	0.964	2648.056	0.975	0.688
P1c	0.930	2239.896	0.860	0.582
P1d	1.160	1910.324	0.657	0.496
P1e	0.858	1991.327	0.749	0.517
Average	0.973	2237.499	0.842	0.581
S1a	0.832	3086.582	0.870	0.802
S1b	0.767	3602.884	1.205	0.936
S1c	0.890	3882.549	0.839	1.009
S1d	0.776	3316.806	0.890	0.862
S1e	0.885	4053.984	0.681	1.053
Average	0.830	3588.561	0.897	0.932

3.6 Explosion Characteristics of Nano-Aluminium Powder with Ceramic

The explosion characteristics of aluminium dust are the basis of the inhibiting effect analysis. It can be seen from Fig. 11 that each explosion pressure profile consists of an initial stage during which dust was dispersed into the test vessel, a second stage during which the pressure increased (corresponding to combustion of the aluminium), and a third stage associated with decay in pressure. Also, the evolutions of the pressure rising rate are consistent with explosion pressure profiles. The pressure rising rate first rises rapidly and then declines during the pressure rising stage and it remains constant in the pressure decay stage.

Based on Fig. 11(B), the pressure–time profile shows peak pressures, indicating that the chemical interaction between Ag-Al causes a reduction in surface area for the oxidation reaction. For comparison with the explosion when original ceramic foams were used (see Fig. 11(A)), at 500 g/m^3 powder concentration, the maximum explosion pressure (Pmax) value obtained was 0.032 bar for Ag-coated ceramic which showed a much lower Pmax value than that of overpressure from the original ceramics (0.186 bar). Meanwhile, the rate of pressure rise (dP/dtmax) for silver-coated foams increases drastically as the concentration increases. The results demonstrate that silver-coated ceramics attenuate the maximal explosion overpressure drastically, by up to 20% due to the interconnected micro-network structure of the metal-ceramic walls which contributes to quenching of aluminium dust flame and suppressing the overpressure. The point is that the presence of agglomerates in dust clouds of very small particles is not only due to incomplete particle dispersion. In addition, new agglomerates are formed continually by inter-particle collision. Green and Lane [33] named this process coagulation and pointed out that continuous and spontaneous coagulation is one of the most striking characteristics of dust clouds. The particles in the cloud, of whatever substance they are composed, will coalesce or stick together if they make contact. The process goes on continuously so that the effective particle size increases and the particles finally settle out of suspension.

The silver-coated foam has no deformation or damage; thus, it can resist the danger of secondary explosions. That is, the flame wave was trapped in porous media and contacted the wall for a long time, which contributed to the sharp decrease in the number of free radicals involved in combustion and flame quenching. Meanwhile, the feasibility of secondary applications of such foam was directly affected by its density, and there were still large deformations and extensive damage after the explosion, despite its certain barrier capacity under the condition of low density. Consequently, ceramic foam with silver coating performs better with the increase in density due to the presence of the silver NPs deposited on the surface of the foam as well as enhancing the overall strength of the foam.

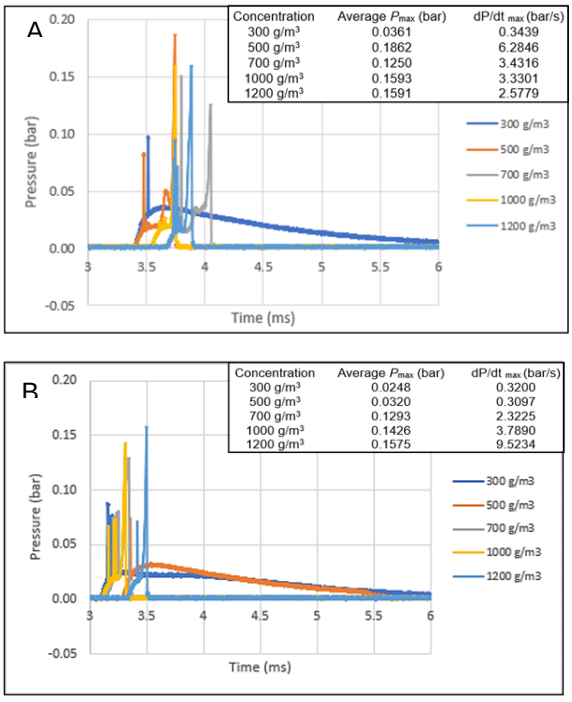

Fig. 11. Pressure–time profile of nano-Al dust explosion at various concentrations (a) with original foam, and (b) with silver-coated foams via spraying method

3.7 Suppression Mechanism of Silver-Coated Ceramic

According to the mechanism diagram of flame propagation shown in Fig. 12(a) and (b), the flame

structure was destroyed by the tiny channel of ceramic foam. The influence of the original ceramic foam on dust flame propagation is comparable to that of silver-coated ceramic foam. As can be seen, the only difference between the two mechanisms is some unburned Al particles might reach the top of the vessel along with some of the burned particles for the explosion when the original foam was used. In this situation in contrast with silver-coated foam, no unburned and burned Al particles reach the venting paper, indicating the effectiveness of the silver coating on the ceramic foam surface in suppressing the explosion much better than those by the original foam. This condition could be supported by the TGA and mechanical test findings for the silver-coated foams. The plateau TG curve begins at 600 °C showed no further weight loss indicating that the silver-coated foams are thermally stable to retain their properties nearly unchanged thus, leading to the enhancement of the foam's strength drastically up to 1 MPa. However, based on the pressure-time profiles for coated foams as shown in Fig. 11(b), the multiple peaks observed might be due to the synergetic effect present between silver metal with aluminium powder. The arrangement of internal spaces within ceramic foam introduces a significant increase in disturbance and interaction when a pressure wave enters the lower surface of the foam. In contrast, it has been observed that silver-coated foam exhibits a superior inhibitory effect on reducing overpressure. This enhanced performance can be attributed to the larger surface area provided by the metallic coating compared to the original foams, thus creating more sites for reactions to occur. Consequently, this leads to the extinguishing of the flame within a specified time frame. As the flame enters the narrow channel, its temperature drops due to the cooling effect of the channel walls, resulting in flame extinction, a phenomenon known as the "cold wall effect". Additionally, the tiny channels within ceramic foam absorb the free radicals generated during the combustion of aluminium powder, subsequently weakening the combustion reaction, referred to as the "wall effect" [34,35]. These two mechanisms, the "cold wall effect" and the "wall effect", respectively, alter the combustion characteristics of the dust flame.

Ceramic foam serves as an effective means to extinguish the deflagration flame resulting from a powder explosion. During the deflagration process, some powder particles in front of the flame wave reach the ceramic foam propelled by the shock wave, and a portion of these particles continue to move through the ceramic foam due to the shock wave's influence. After reaching the ceramic foam, most of the powder particles remain within and on the porous structure, as shown in Figure 12(a) and (b). Some powder does not enter the ceramic foam and remains at the bottom of the vessel. Afterwards, the flame seems to reside on the surface of the ceramic foam and fails to penetrate it, and is eventually extinguished. This phenomenon is commonly referred to as porous media quenching and similar occurrences have been observed in previous experiments [36,37]. As Ciccarelli et al. [38] explained, the porous media extracts energy from the passing flame, thereby reducing the flame temperature and hence quenching it. The unique porous structure of ceramic foam divides the space into several small areas, which will divide the deflagration flame into several small flames [39], thereby dispersing the energy generated by deflagration and weakening the combustion reaction. Ceramic foam, particularly made of alumina possesses good heat resistance and heat insulation properties. The heat generated during the deflagration is isolated by the porous structure's strong insulating effect, leading to a decrease in the flame front's temperature and preventing flame propagation. Once the heat dissipation due to the wall effect surpasses the heat released by the deflagration, the flame is extinguished [34]. Furthermore, the ceramic foam's porous structure obstructs unburned and burning powder particles, disrupting the fuel supply and thus interrupting the reaction. In fact, metals, when burnt in oxygen, form their oxides which are basic in nature. In order to understand the mechanism better, the overall chemical reactions for the Al powder explosion of (a) with ceramic foam, and (b) with silver-ceramic foam were expressed in the diagram below:

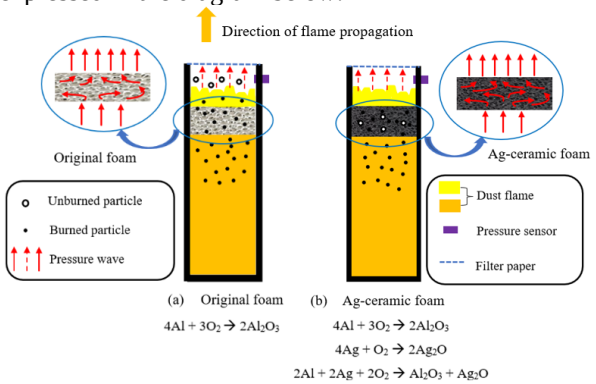

Fig. 12. Flame propagation mechanism in (a) original foam, and (b) silver-ceramic foam

4 Conclusion

In this study, the explosion characteristics of nano-aluminium dust explosion, which was suppressed by silver nanoparticles (Ag NPs) coated on ceramic foam were experimentally investigated. The main conclusions are as follows:

1) The use of APTMS as a surface modifier resulted in a strong and thin coating layer of Ag NPs on the surface of the ceramic.
2) The pre-explosion and post-explosion analysis for the silver-coated foams were done by comparison with the original foam. It showed that the ceramic foam with the silver coating outperformed the original foam in terms of its mechanical strength, thermal stability, and robustness in lowering the explosion overpressure during the aluminium powder explosion.
3) It was found that the percentage increase of maximum load for silver-ceramic foam from the original ceramic foam was about 60%. The results indicate that silver-ceramic has a better

compressive strength of 0.93 MPa as compared to 0.58 MPa by the original ceramic.

4) The silver-coated ceramic foam exhibited a 15% reduction in maximum pressure (P_{max}) compared to the original ceramic foam. However, achieving a uniform and well-distributed particle coating on the surface proved to be a challenge.
5) Observation revealed multiple pressure peaks when the coated ceramic foam was subjected to aluminium powder explosion. This indicates that the interaction between Ag and Al reduces the surface area available for oxidation, resulting in fewer free radicals participating in the reaction. The coated ceramic foam mitigates flame propagation fluctuations by suppressing turbulence and effectively quenching deflagration flames generated from aluminium powder explosions.

In conclusion, silver-coated ceramic foam demonstrated promising results in reducing overpressure and suppressing flame propagation. Ag NPs coating on the surface of the ceramic foam has a significant effect on the deflagration flame propagation behavior in aluminium powder explosions. This has certain potential for application in the flameless venting of dust explosions in various industrial processes. Overall, the silver-coated ceramic foam decreases the fluctuations in flame propagation acceleration due to its weakening of the turbulence therein as well as the presence of heterogeneous interaction between aluminium fuel and silver powder coating on the ceramic foam at maximum explosion pressure. Study results cannot only further explain the essence of dust explosion and its propagation, but also reduce the intensity of dust explosion accidents. In addition, it will also play a positive role in enriching and perfecting the theory of a dust explosion. The outcomes can also be extended to other industries such as explosion suppression, explosion proof, explosion extinguishment and other safety fields, so it has a high academic value and wide application prospects.

The authors would like to express their appreciation for the funding assistance of the sponsors – Ministry of Higher Education Malaysia (MOHE) under the Fundamental Research Grant Scheme (FRGS) (FRGS/1/2020/STG07/UTM/02/6), and Universiti Teknologi Malaysia under a Collaborative Research Grant (Q.J130000.2451.08G95).

References

1. R. K. Eckhoff, Dust explosions in the process industries. J. Hazard. Mater. **54**, 266–267 (1991)
2. K. L. Cashdollar, M. Hertzberg, Industrial dust explosions. Lancet. **181**, 121–121 (1987)
3. Li, G., Yang, H.-X., Yuan, C.-M., Eckhoff, R. K., A catastrophic aluminium-alloy dust explosion in China. J. Loss. Prevent. Proc. **39**, 121–130 (2016)
4. T. Zhang, H. Jiang, S. Shang, K. Zhang, W. Gao, Synthesis of aluminum hydroxide/Zinc borate composite inhibitor and its inhibition effect on aluminum dust explosion. Chem. Eng. Sci. **248**, 117204 (2022)
5. T. Abbasi, S.A. Abbasi, Dust explosions–Cases, causes, consequences, and control. J. Hazard Mater. **140**, 7-44 (2007)
6. G. Li, H.-X. Yang, C.-M. Yuan, R.K. Eckhoff, A catastrophic aluminium-alloy dust explosion in China. J. Loss Prev. Process Ind. **39**, 121-130 (2016)
7. H. Dai, X. Wang, X. Chen, X. Nan, Y. Hu, S.He, B. Yuan, Q.Zhao, Z. Dong, P. Yang, Suppression characteristics of double-layer wire mesh on wheat dust flame. Powder Technol. **360**, 231-240 (2020)
8. N. Kuai, J. Li, Z.Chen, W. Huang, J. Yuan, W. Xu, Experiment-based investigations of magnesium dust explosion characteristics. J. Loss Prev. Process Ind. **24**, 302-313 (2011)
9. N. Kuai, W. Huang, B. Du, J. Yuan, Z. Li, Y. Gan, J. Tan, Experiment-based investigations on the effect of ignition energy on dust explosion behaviors. J. Loss Prev. Process Ind. **26**, 869-877 (2013)
10. A. Di Benedetto, P. Russo, P. Amyotte, N. Marchand, Modelling the effect of particle size on dust explosions, Chem. Eng. Sci. 65, 772-779 (2010)
11. C. Kauffman, Agricultural dust explosions in grain handling facilities. Fuel-air. Explos. 305–347 (1982).
12. W. L. Frank, Dust explosion prevention and the critical importance of housekeeping. Process Saf. Prog. **23**, 175–184 (2004)
13. C. Huang, X. Chen, B. Yuan, H. Zhang, S. Shang, Q. Zhao, H. Dai, S. He, Y. Zhang, Y. Niu, Insight into suppression performance and mechanisms of ultrafine powders on wood dust deflagration under equivalent concentration. J. Hazard Mater. **394**, 122584 (2020)
14. Q. Zhao, X. Chen, H. Dai, C. Huang, J. Liu, S. He, B. Yuan, P. Yang, H. Zhu, G. Liang, B. Zhang, Inhibition of diammonium phosphate on the wheat dust explosion. Powder Technol. **367**, 751-761 (2020)
15. X. Chen, H. Zhang, X. Chen, X. Liu, Y. Niu, Y. Zhang, B. Yuan, Effect of dust explosion suppression by sodium bicarbonate with different granulometric distribution. J. Loss Prev. Process Ind. **49**, 905-911 (2017)
16. Gauckler, L.J., Waeber, M.M., Conti, C., M. Jacob-Duliere, Ceramic Foam for Molten metal Filtration. JOM **37**, 47–50 (1985)
17. E.A. Dawson, P.A. Barnes, M.J. Chinn, Preparation and characterisation of carbon-coated ceramic foams for organic vapour adsorption. Carbon. **44**, 1189-1197 (2006)
18. M V. Twigg, J.T. Richardson, Fundamentals and Applications of Structured Ceramic Foam Catalysts. Ind. Eng. Chem. Res. **46**, 4166–4177 (2007)
19. B. Nie, X. He, R. Zhang, W. Chen, J. Zhang, The roles of foam ceramics in suppression of gas

explosion overpressure and quenching of flame propagation. J Hazard Mater. 192, 741-747 (2011)
20. J. Zhang, Z. Sun, Y. Zheng, Z. Su, Coupling effects of foam ceramics on the flame and shock wave of gas explosion. Safety Science. **50**, 797-800 (2012)
21. L. Pang, C. Wang, M. Han, Z. Xu, A study on the characteristics of the deflagration of hydrogen-air mixture under the effect of a mesh aluminum alloy J Hazard Mater. **299**, 174-180 (2015)
22. K.M. Mokhtar, R.M. Kasmani, C.R.C. Hassan, M.D. Hamid, M.I.M. Nor, N. Ibrahim, Study of the Explosibility Characteristics of Aluminium-Silver Metal Mixtures. Combust. Sci. Technol. **192**, 885–901 (2019)
23. Y. Luo, Y. Jiang, J. Zhu, J. Tu, and S. Jiao, Surface treatment functionalization of sodium hydroxide onto 3D printed porous Ti6Al4V for improved biological activities and osteogenic potencies. J Mater Res Technol. **9**, 13661-13670 (2020).
24. S. Chandren, B. Ohtani, Preparation and reaction of titania particles encapsulated in hollow silica shells as an efficient photocatalyst for stereoselective synthesis of pipecolinic acid. Chem. Lett. **41**, 677–679 (2012)
25. N.F. Hamzah, R.M. Kasmani, S. Chandren, N. Ibrahim, A.A. Jalil, Effect of metal coating on physicochemical properties of ceramic foam for flame suppression application. Ceram Int. (2023)
26. K.M. Mokhtar, R.M. Kasmani, C.R.C. Hassan, M.D. Hamid, M.I.M. Nor, M.U.M. Junaidi, N. Ibrahim, Nanometal Dust Explosion in Confined Vessel: Combustion and Kinetic Analysis. ACS Omega. 6 (2021)
27. W. Gao, X. Zhang, D. Zhang, Q. Peng, Q. Zhang, R, Dobashi, Flame propagation behaviours in nano-metal dust explosions. Powder Technol. 321, 154-162 (2017)
28. J. Sun, R. Dobashi, T. Hirano, Structure of flames propagating through aluminum particles cloud and combustion process of particles. J. Loss Prev. Process Ind. 19, 769-773 (2006)
29. J. Bouillard, A. Vignes, O. Dufaud, L. Perrin, D. Thomas, Ignition and explosion risks of nanopowders. J Hazard Mater. 181, 873-880 (2010)
30. M. Mittal, Explosion characteristics of micron- and nano-size magnesium powders. J. Loss Prev. Process Ind. **27**, 55-64 (2014)
31. P. Prakash, P. Gnanaprakasam, R. Emmanuel, S. Arokiyaraj, M. Saravanan, Green synthesis of silver nanoparticles from leaf extract of Mimusops elengi, Linn. for enhanced antibacterial activity against multi drug resistant clinical isolates. Colloids Surf B: Biointerfaces. **108**, 255-259 (2013)
32. H. Yu, Z. Guo, B. Li, G. Yao, H. Luo, and Y. Liu, Research into the effect of cell diameter of aluminum foam on its compressive and energy absorption properties. Mater. Sci. Eng. A. **454**, 542–546 (2007)
33. H. L. Green, & W. R Lane, Particulate clouds: Dusts, smokes and mists (2nd ed.). London. Belfast: E. & F.N. Spon Ltd., Printed by The University Press (1964)
34. N. Iida, O. Kawaguchi, G.T. Sato, Premixed flame propagating into a narrow channel at a high speed, part 1: flame behaviors in the channel. Combust. Flame. **60**, 245–255 (1985)
35. M.I. Radulescu, J.H.S. Lee, The failure mechanism of gaseous detonations: experiments in porous wall tubes. Combust. Flame. **131**, 29–46 (2002)
36. H.I. Joo, K. Duncan, G. Ciccarelli, Flame-quenching performance of ceramic foam, Combust. Sci Technol. **178**, 1755-1769 (2006)
37. B. Nie, X. He, R. Zhang, W. Chen, J. Zhang, The roles of foam ceramics in suppression of gas explosion overpressure and quenching of flame propagation. J Hazard Mater. **192**, 741–747 (2011)
38. G. Ciccarelli, C. Johansen, M. Parravani, Transition in the propagation mechanism during flame acceleration in porous media. Proc. Combust. Inst. **33**, 2273–2278 (2011)
39. Q. Zhao, H. Dai, X. Chen, C. Huang, H. Zhang, Y. Li, S. He, B. Yuan, P. Yang, H. Zhu, G. Liang, B. Zhang, Characteristics of wheat dust flame with the influence of ceramic foam. Adv. Powder Technol. **31**, 3570–3581 (2020)